 doi:10.20944/preprints202205.0273.v1

Article

Detection of Irrigated Permanent Grasslands with Sentinel-2 based on temporal patterns of the Leaf Area Index (LAI).

Mukhtar Abubakar, André Chanzy*, Guillaume Pouget, Flamain Fabrice, Dominique Courault

1114 UMR INRAE-Avignon University EMMAH, Domaine St. Paul, 84914, Avignon, France

* Correspondence: andre.chanzy@inrae.fr

Abstract: Conventional methods of crop mapping need ground truth information to train the classifier. Thanks to the frequent acquisition allowed by recent satellite missions (Sentinel 2), we can identify temporal patterns that depend on both phenology and crop management. Some of these patterns are specific to a given crop and thus can be used to map it. Thus, we can substitute ground truth information used in conventional methods with agronomic knowledge. This approach was applied to identify irrigated permanent grasslands (IPG) in the Crau area (Southern France) which play a crucial role in groundwater recharge. The grassland is managed by making three mows during the May-October period which leads to a specific temporal pattern of leaf area index (LAI). The mowing detection algorithm was designed using the temporal LAI signal derived from Sentinel 2 observations. The algorithm includes some filtering to remove noise in the signal that might lead to false mowing detection. A pixel is considered a grassland if the number of detected mows is greater than 1. A data set covering five years (2016-2020) was used. The detection mowing number was done at the pixel level and then results are aggregated at the plot level. A validation data set including 780 plots was used to assess the performances of the classification. We obtained a Kappa index ranging between 0.94-0.99 according to the year. These results were better than other supervised classification methods that include training data sets. The analysis of land-use changes shows that misclassified plots concern grasslands managed less intensively with strong intra-parcel heterogeneity due to irrigation defects or year-round grazing. Time series analysis, therefore, allows us to understand different management practices. Real land-use change in use can be observed, but long time series are needed to confirm the change and remove ambiguities with heterogeneous grasslands.

Keywords: irrigation, remote sensing, Sentinel-2, grasslands, leaf area index, land use classification

1. Introduction

According to United Nations [1], water is a scarce resource thus, its justifiable and judicious use must remain a crucial and fundamental target for sustainable developments across the globe, especially in a world with a constantly increasing populace that directly or indirectly depends on this scarce resource for sustaining their activity and food production system. Undoubtedly agriculture remains an obvious focal point in water management, as the main water user [2], irrigation accounting at world-scale about 70% of the global freshwater withdrawals [3]. The effect of global changes is anticipated to heighten the issue of water shortage and irrigation needs [4]. Thus, attention is needed on appraisals related to irrigation activities to bolster water resource management, maximize water productivity and boost agricultural water sustainability [5]. To match water needs and resources, better planning is needed for irrigation activities [6]. One of the key solutions to good irrigation planning is the provision of extensively detailed spatial delineations of croplands under irrigation [7] and the description of irrigation systems and strategies that may lead to

 doi:10.20944/preprints202205.0273.v1

various water needs across the year [8]. There is therefore a challenge to detect not only the irrigated areas but also the associated production systems.

The classification of irrigated areas is widely discussed in the literature [8]. While the use of medium resolution satellites has allowed the establishment of methodological bases applicable to regional scales, there is a renewed interest in these methods with the Sentinel satellites, which offer both good temporal repeatability (3-5 days) and good spatial resolution (10m), which is particularly relevant for crop monitoring. Classification methods for irrigated surfaces are generally based on radar data giving temporal series of surface moisture, data in the optical domain with monitoring of vegetation dynamics, and meteorological data. The use of optical data to separate irrigated and non-irrigated areas is based on the green cover dynamic which displays higher level when additional water is brought to the crop. According to [9], they identified anomalies in vegetation development during periods of climatic water stress and use this information to inform a decision tree. The authors of [10] make a classification on the temporal characteristics of the vegetation signal such as the maximum and the range of variation of the vegetation index. They showed as in [9] that the Green Index (GI) is the best vegetation index. Moreover, the accuracy of the classification can be improved with additional information as the aridity index derived from climatic data. It is important to note that the use of temporal features rather than images times series has reduced the training efforts. For instance, in [9] a training made on a wet and a dry year is enough to be implemented on all years. In recent years the combined use of radar Sentinel-1 and optical Sentinel-2 has shown a moderate improvement in classification [5, 11, 12] when compared to method based on Sentinel-2 only. The authors of [13] went further by analysing the radar time series to detect irrigation events, which are then used to determine automatically a corpus of control points for both the irrigated and the non-irrigated classes. Then they used a classical supervised classification using the Random Forest method on both radar and optical images. The use of radar data alone gives excellent results in Catalonia [5] while in the South-West of France the performance is less good with Overall accuracy > 70% and kappa of 0.89 [11, 12]. The authors of [5] showed that it is possible to separate irrigation systems between crops and orchards based on the variability of the radar signal and the temporal autocorrelation length of this signal. Both [6] and [10] show that consideration of agronomic traits related to phenology and cropping interventions can provide information used to characterize irrigated systems. The Sentinel 2 temporal revisit opens doors to carry out such analyses and to exploit them to classify the areas.

Multitemporal data can be used to map crop conditions, agronomic activities, and phenology of plots under irrigation that can serve as added information for decision making [14]. For instance, [15] made a classification of canola fields in Iran and the United States of America (USA) by proposing a new index (canola index) based temporal changes in the green and red band that are linked to some agronomic activity (harvest) and phenological features (flowering period). The comparison with conventional classification approaches like Maximum Likelihood (ML) and Support Vector Machine (SVM) have shown the interest of using agronomic traits to identify a given crop with an improved accuracy. A similar attempt was established in extensive agricultural fields to separate potato field classes from other crop classes by [16]. The authors based their mapping criteria on spectral indices linked to phenological (flowering and peak of greenness) and agronomic traits (harvesting periods of early and late potato fields) leading to good classification accuracy (Kappa~0.8) with little training. The authors of [17] made a land-use map based on the annual behaviour of both the land surface temperature (LST) and the NDVI. The classification was performed on characteristics of the LST/NDVI yearly relationship and produce good results for the identification of irrigated fields (kappa=0.85).

 doi:10.20944/preprints202205.0273.v1

In the work reported here, we wished to develop a method dedicated to irrigated permanent grass (IPG), which is irrigated using flooding techniques. Such practice has a strong impact on the regional water budget by consuming a very large amount of water (about 20000 m^3/ha/year [18]) but also provides important externalities such as the groundwater recharge. IPG detection is an interesting case as it provides very clear agronomic traits with several mowing events across the year that can be used for the classification. The characterisation of grasslands has already been the subject of several studies. The authors of [19] showed that with a limited number of SPOT images (3 in the study) one can separate mown grasslands from grazed grasslands with a kappa=0.82. In this study, it was also found that LAI is the best indicator to make such a distinction. More recently the authors of [20] classify grassland use intensity with 5 rapid eyes images based on the variability of the temporal signal. A similar approach was followed by [21] who use a series of 14 Landsat dates to distinguish 6 classes of grassland reflecting different management strategies. These results announce the potential of Sentinel-2, which was used to detect mowing events [22, 23]. All the proposed methods are based on frequent temporal sampling and local minimum detection. The algorithms differ in principle but are designed to avoid false detections by relying on thresholds on vegetation index variations before or after mowing detection. It should be noted that these characterisations are done on known grassland areas and are not used for the classification of grassland areas. It should also be noted that the scores show difficulties to detect unambiguously all mowing events with an overall accuracy of 72% [22] or a F-score of 0.60 [23].

In this study, we developed a classification method to map IPG in South-East France, which present specific temporal pattern linked to a specific agronomic trait that is a number of mowing events greater than one. The approach was developed in the context of the Crau area in Southern France in the Mediterranean. IPG are both an emblematic crop of the areas and plays an important role in the superficial aquifer water budget [18]. In this paper, we develop a mowing event algorithm able to minimise false mowing event detection and account for temporal sampling of Sentinel-2 data that may present missing observation dates during mowing periods. The classification performance was compared to the traditional classification method made directly on vegetation indices time series and the THEIA product, which is an operational product implemented over France. Five classifications made during the 2016-2020 period were analysed. Misclassified plots were carefully analysed to understand the origin of errors and thus lessons we can learn about the limitations of the method.

Preprints (www.preprints.org) | NOT PEER-REVIEWED | Posted: 20 May 2022 doi:10.20944/preprints202205.0273.v1

2. Materials and Methods

2.1 The study site

Crau region (Fig. 1) is located at 43°38 N, 5°00 E (5 m a.s.l), near the Rhône delta in Southern France which covers a surface area of 540 to 600 km^2. The climate of the Crau region is Mediterranean with an average annual rainfall of 600 mm (non-uniform) and a potential evapotranspiration of 1100 mm. Mean air temperature of about 7-8°C (in winter) and 24°C (in summer) [22,24]. The Crau region is characterised by native shallow soils of about 60-80 cm with 90% stones consequently rendering its water retention very low. Soils irrigated using flooding technics present a loamy surface soil layer thanks to sediments transported via irrigation water with a layer depth that can reach 60 cm depending on the length of the irrigation period [22]. IPG are the most predominant irrigated crops in the Crau area [18, 22] with a coverage of about 13000 ha (23%) as depicted in Fig.1 (the dark green plots). The irrigation practice of permanent grasslands in the Crau region is more than 4 centuries old which can be dated back to the 16th century [24]. The common practice mostly remains the same which involves the use of gravity (flood) for irrigation, on areas specifically dedicated to hay production and rearing of sheep. The water used for flooding irrigation contribute to more than 75% of the groundwater table. This ground water table is used for irrigation of intensive orchard and market garden productions, domestic and industrial purposes to roughly 280,000 people around the southern part of the area [22,24]. Duration for irrigation in a year extends to about seven months [18] from March to September. IPG management is regulated by the selling label *"foin de Crau"* the first COP (Certified Origin Product) in France leading to standardize management with three or four grass mowings from May 1st to the end of October and sheep grazing in winter. In general grass fields are irrigated optimally to cover the water needs but, in some places, and some years the access to water might be critical thus leading to reduce grass productivity and skipping a mowing operation. Some farmers do not follow the label rules, for example when they breed animals all year round, which leads to a different spatial and temporal dynamics of the vegetation cover than the one obtained with the recommended cultivation practices, which are dominant on the territory. The grass fields are in general homogeneous but heterogeneities in vegetation cover were found at the field boarder or within the field when surface levelling is not satisfactory generating heterogeneities in the water supply. Therefore, if a dominant grass development temporal pattern is expected and then used to identify grassland areas, the mentioned variation can interfere with the classification process.

Preprints (www.preprints.org) | NOT PEER-REVIEWED | Posted: 20 May 2022 doi:10.20944/preprints202205.0273.v1

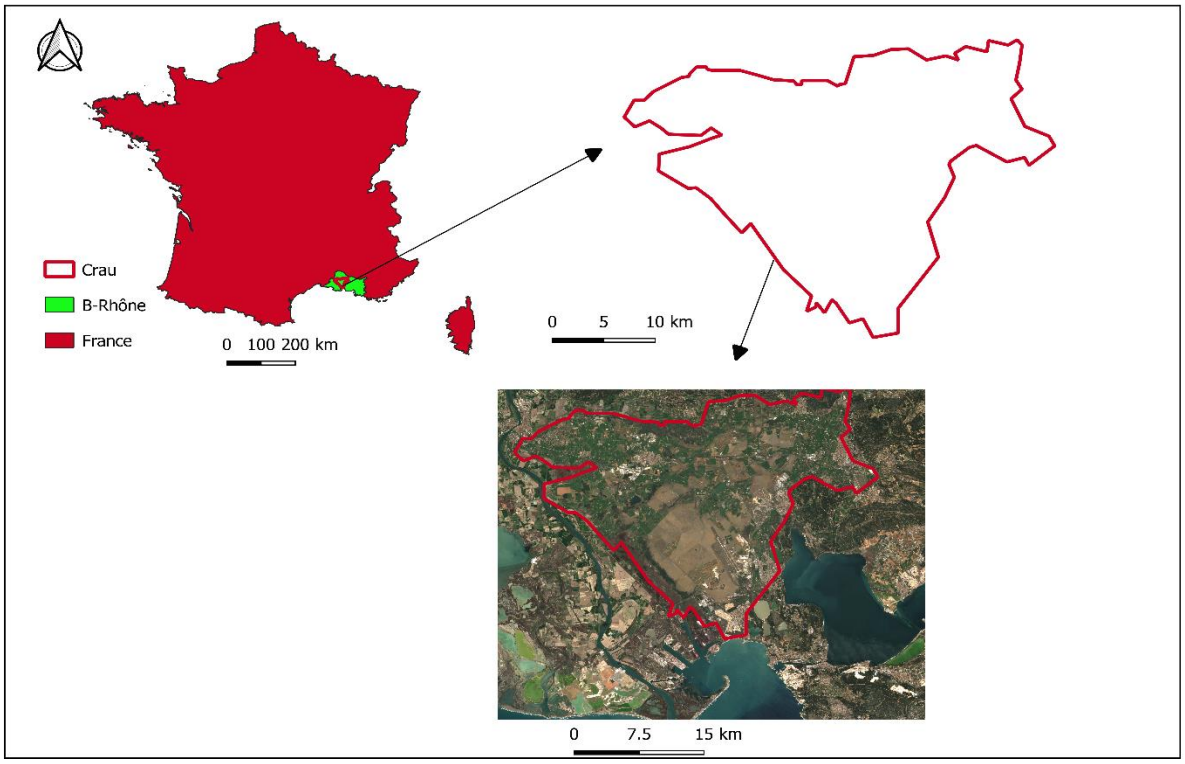

Figure 1. Study site location

2.2 Data used

2.2.1 Field survey

A field survey was done to identify crop type and irrigation over a total of 809 plots (all plots were greater than 1 ha) by a visit done during the 2016-2020 periods. During the visit, surveyed plots were identified and observed crop were reported in the plot map established over the whole area. Irrigated permanent grasslands (IPG) consisted of 391 plots and Not Irrigated Grasslands (NIG) comprise 418 plots. In addition, aerial photographs were used to check management features such as soil levelling, land-use change, or grazing. For that purpose, we used Google Earth images acquired during the 2015-2021 period together with the IGN (the French National Geography Institute) 2020 flight campaign. Plot boundaries were drawn in 2012 throughout the Crau area based on cadastre and photo interpretation leading to a total of 18058 plots.

2.2.2 Satellite data

Time series of Sentinel-2 of level 2A optical images were used for this study, which were collected from both Sentinel-2A and Sentinel-2B for all dates from 2016 to 2020. We used the images distributed by the french land data open-source service center (https://www. theia-land.fr/), which also propose cloud masks that were used to remove pixels affected by clouds. The number of remaining dates during the considered period (March 15th to October 30th) are given in Table 1. As Sentinel 2B satellite was operational during 2017 we got less date in 2016 and 2017. The number of availables dates varied in the image due to occurrence of cloud which was not homogeneous within the Crau area.

Preprints (www.preprints.org) | NOT PEER-REVIEWED | Posted: 20 May 2022 doi:10.20944/preprints202205.0273.v1

Table 1: Statistics on the number of days available over the period from 15 April to 30 October after removing the dates impacted by clouds. The filtering is carried out at the pixel level and the statistics have been calculated on all the pixels of the Crau

Year	Average	maximum	minimum
2016	26	31	20
2017	43	49	37
2018	52	61	44
2019	54	59	48
2020	49	56	42

The BVNET model using bands 3, 4 and 8 was used. It is based on neural network trained on simulated spectral reflectance using a radiative transfer model [25]. Temporal profiles of leaf area index (LAI) were then established for each 10 meters pixels.

2.2.3 Benchmark

Different existing classification methods based on Sentinel 2 data were considered to assess the adding value of the new proposed method described above. First, we have used a supervised classification based on Support Vector Machine (SVM) method, which is rather common and powerful to discriminate two classes. The approach was implemented using thirty-seven (37) cloud-free images for 2016 and forty-four (44) cloud-free images for 2017 using normalized difference vegetation index (NDVI) with 60 plots of ground reference. Such an approach does not take profit on the temporal behaviour of the vegetation patterns explicitly.

We also consider the THEIA land use map as a benchmark since it is implemented yearly over the whole national territory (https://www.theia-land.fr/ceslist/ces-occupation-des-sols/). It is a supervised classification [26] based on random forest classifications using all Sentinel-2 dates and the VIS and NIR bands and as auxiliary information the RPG (‘registre parcellaire graphique) data which gathers farmer’s annual declarations to get subsidies from the European Union. Seventeen classes were identified with one dedicated to grasslands.

2.3. Developed irrigated grassland detection algorithm.

The specificity of irrigated grasslands is that they present several mowing-vegetation growth cycles during the year. To detect a grassland, we can also rely on the level of LAI, which is generally high (LAI >4) when the vegetation is well developed, and the growth rate after a cut which is specific to grassland. For example, in the study area, it takes 30 to 50 days after a cut to return to a vegetation development comparable to that before the cut. Although these characteristics specific to irrigated grassland should make it relatively easy to identify them with a temporal sampling such as that offered by the Sentinel-2 mission, we were confronted in the time series with LAI variations linked to atmospheric corrections that may generate temporal patterns of LAI leading to confusion with grassland mowing events. In addition, the presence of clouds during the mowing periods reduces the time sampling of the LAI that prevents a clear detection of a mowing event.

Preprints (www.preprints.org) | NOT PEER-REVIEWED | Posted: 20 May 2022 doi:10.20944/preprints202205.0273.v1

As in [23] and [27], the detection algorithms of mowing events developed in the study are based on a sharp reduction in vegetation amount followed by a significant vegetation development during the following 45 days. To monitor the development of vegetation, we used the LAI estimated from Sentinel 2. This choice is justified by the desire to have a quantity that is more sensitive to variations in well-developed vegetation while conventional vegetation indices tend to saturate more easily [27]. The algorithms have shown their quality for homogeneous vegetation covers such as cereal or grassland covers. The disadvantage is that the computed LAI are more sensitive to atmospheric corrections as we no longer have the normalization of measurements made on classical vegetation indices such as the NDVI. On the other hand, on some surface types, the LAI inversion algorithm may fail. For example, we found very high and variable LAI values on greenhouses with a non-negligible risk of confusion with grasslands. These inconveniences lead to the implementation of tests on the time series to identify a mowing event among others.

To detect an irrigated grassland, we made the following main assumptions:

1) There are at least 2 mowing events during the May to October period. If most of the irrigated grassland is managed with 3 or 4 mowing events, this threshold makes it possible to consider less intensively managed grasslands or to allow for the possibility of missing a mowing event due to an unfavourable time series with a long cloudy period during the mowing period. Such a situation can happen even in the Mediterranean area despite the high revisit frequency of the sentinel-2 satellites.
2) A mowing event is characterized by a local minimum with significant variations in LAI over 45 days before and after this minimum. The period of 45 days after the minimum reflects the growth time of the grassland after mowing. The period of 45 days before may seem long since a mowing induces an immediate drop in the amount of vegetation. However, we found that some mowings were delayed and then the grassland began to senesce, resulting in a decrease in green leaf area as captured by the LAI estimate. A shift of 10 to 20 days in the maximum LAI before mowing can thus be observed. In addition, gaps in LAI time series may lead to the maximum being sought over a somewhat longer period.

To implement these assumptions, we propose a five steps algorithm as summarized in Figure 2

Step 1: we first flagged the LAI time series by considering that the maximum LAI must be greater than *tlaimin* and lower than *tlaimax*. *tlaimin* threshold reflects the fact that irrigated grassland leads to strong vegetation development while *tlaimax* is dedicated to eliminating surface type on which the LAI computation fails leading to unrealistic high values.

Step 2: To eliminate local minimum due to short-term LAI variations as induced by poor atmospheric corrections, different smoothing procedures were presented in [28]. In this work we used the smooth spline algorithm in R [29], which is efficient and flexible. The algorithm involved a degree of freedom parameter (*df*) controling the smoothing process. The minimum was then detected on the smoothed LAI time series that might be slightly delayed in comparison to the date of the corresponding minimum in the raw LAI time serie.

Step 3: Some remaining anomalies in the LAI time series that might impact the LAI variations computation will be corrected. When the LAI is too small, i.e lower than *tlailow* or when the difference between the observed LAI and the smoothed LAI is greater than *difmax*, the observed LAI is substituted by the corresponding smoothed LAI value.

Preprints (www.preprints.org) | NOT PEER-REVIEWED | Posted: 20 May 2022 doi:10.20944/preprints202205.0273.v1

Step 4: every detected minimum in step 2 is validated according to different criteria. First, the date of the observed minimum (*tmin*) is searched in the raw LAI time serie within a time window around the minimum detected on the smoothed signal. This time window ranges from *dtb1* days before and *dta1* days after the date of the minimum detected in step 2. The time *tmin* must fall within the considered period starting at *dbeg* and ending at *dend*, being in our case May 1st and October 15th, respectively. Then the value of the minimum was analyzed. We consider that the minimum LAI must be lower than a threshold, this threshold being adapted according to the LAI sampling date before and after the minimum date. Indeed, if the LAI is sampled loosely around the minimum, the truncation effect of the time series may result in a minimum value that is larger than the true minimum, as the vegetation may have started to grow at the time of the measurement. The threshold is therefore set according to the following relationship:

tminlai= tminlai0 when *dt<dtmin0*

tminlai=tminlai1 when *dt> dtmin1*

$$tminlai = tminlai0 + {}^{dt}/_{(dtmin1 - dtmin0)} \cdot (tminlai1 - tminlai0) \quad (1)$$

with *dt* being the time interval between the first acquisition dates before and after *tmin*. If the minimum is validated (*LAI(tmin)<tminlai*), the last test was done on the LAI variations before (within the [*tmin-dtb – tmin*] period and after (within the [*tmin– tmin+dta*] period) that must be greater than *threshlai*. The period before the minimum is reduced when the LAI sampling is tightened. If the measurement period of the *nbb* observations before the minimum is shorter than *dtb* then this period is used to calculate the LAI variation.

Step 5: The number of validated minimums, considered as mowing events, is established and used to apply the irrigated grassland filter being a minimum of two events.

The algorithm is applied at the pixel level. However, due to plot heterogeneity or border effect, an aggregation was done within the plot boundary after applying a buffer of 20 m. Then a plot was declared as irrigated grassland when a majority of pixels were classified as irrigated grassland, the majority being qualified by a percentage of the pixel that has to be determined (*pixperc*).

Preprints (www.preprints.org) | NOT PEER-REVIEWED | Posted: 20 May 2022 doi:10.20944/preprints202205.0273.v1

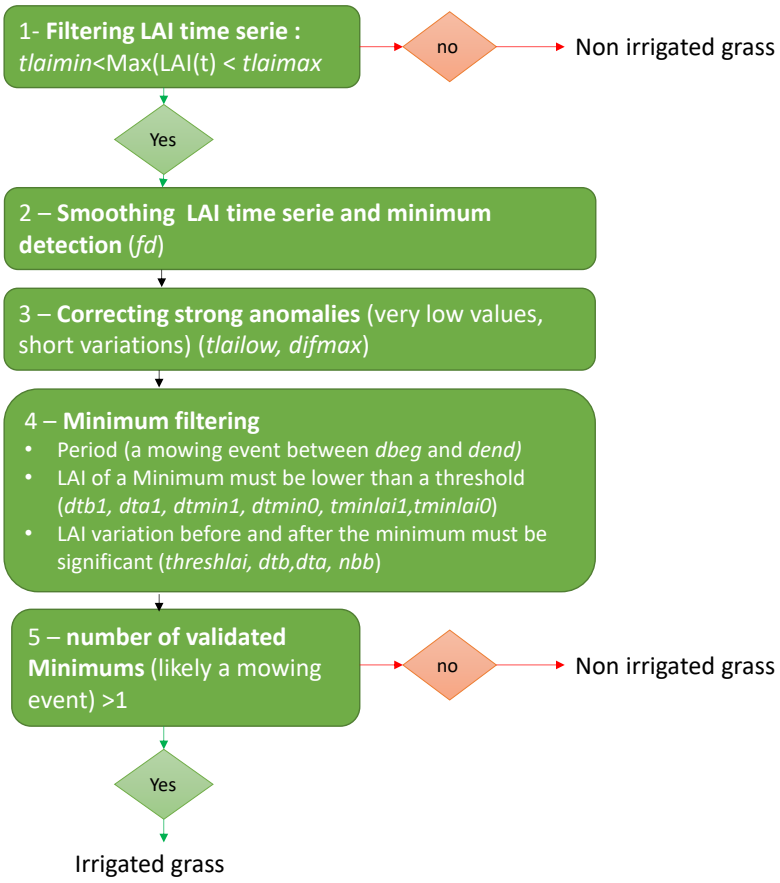

Figure 3 : Five steps of the developed irrigated grassland algorithm

The detection algorithm involved 16 parameters that are summarized in Table 2. As the number of parameters was large we prescribe some of them to values consistent with our agronomical knowledge while the other parameters were calibrated.

2.4 Calibration and Validation

The calibration procedure targeted the best parameters to be used for the separation of IPG from NIG. The calibration was done considering 29 vignettes surrounding an IPG plot. In each vignette we determined 6 polygons, 3 being inside the grassland plot and three being outside (Figure 3) corresponding to surfaces that might be orchards, vineyards, field crops, market gardens, dry grasslands... Each polygon is considered as a single entity on which metrics describing the mowing event number distribution are computed.

Preprints (www.preprints.org) | NOT PEER-REVIEWED | Posted: 20 May 2022 doi:10.20944/preprints202205.0273.v1

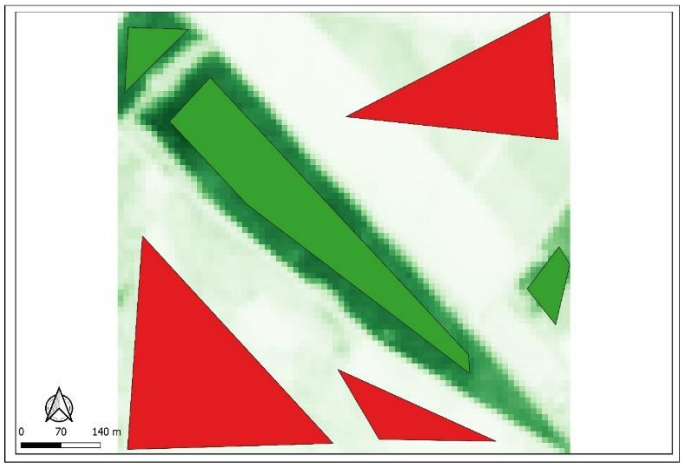

Figure 3 : green polygons symbolise IPG while red polygons symbolise NIG

The cost function used for calibration was the percentage of well-classified polygons i.e that having a majority of pixels with at least 2 mowing events for the IPG IPG polygons and lower than 2 for the NIG polygons. A database covering the 2016-2020 period was generated, considering that every year provides a set of data to compute the cost function.

Two phases are considered in the calibration. First, based on agronomic knowledge and/or visual analysis of LAI time series, we set *dta* and *dtb* to 45 days, *dta1 to 15* days, *dtb1 to 25* days and *dbeg* and *dend* set to may 1st and Octobr 15th, respectively. Then *fd, tlaimax, tlaimin, threslai,* and *pixperc* were calibratedusing a manual fitting considering the range of value given in Table 2. In that first calibration phase, the LAI anomaly correction (step 3) and the filtering tests on the minimum value (step 4) involving the other parameters were not activated.

Then, in a second phase, some refinements were added to the minimum detection algorithm *dtlimlai0, dtlimlai1, dtmin0, dtmin1, and tlailow* were prescribed to 15, 25, 10, 25, 2, 2.5, and 0.4, respectively, based on the visual analysis of LAI time series that led to an error in phase 1. The other parameters (*difmax, nbb*) were calibrated.

The validation was made on 780 plots not used for the calibration with 362 IPG plots and 418 NIG plots which in detail their break down goes as 162 orchards; 100 vineyards; 99 greenhouses; 20 dry grass; 33 field crops and 4 lawns.

2.5 Accuracy assessments

Accuracy assessments during validation remain an important aspect of mapping projects utilizing remotely sensed information [30]. The different classifications made in the study were evaluated using the overall accuracy (OA), the producer's accuracy (PA), and Cohen's Kappa index (K), all quantities being derived from the confusion matrix having the following terms: TG (well-classified irrigated grassland plots) , FG (plot classified as irrigated grassland while not an irrigated grassland), TNG (well classified not irrigated grassland plots), FNG (irrigated grassland plot classified as not irrigated grassland).

$$Overall\ accuracy = \frac{\mathrm{TG+TNG}}{TG+FG+TNG+FNG} \cdot 100 \qquad 2$$

Preprints (www.preprints.org) | NOT PEER-REVIEWED | Posted: 20 May 2022 doi:10.20944/preprints202205.0273.v1

Producer's accuracy corresponds to the error due to omission (exclusion). From the perspective of the land use map maker, it indicates how accurate is the map : for a given class, how many plots among the reference plots in the map were tagged accurately. It is defined for the IPG as ;

$$Producer's\ accuracy = \frac{\mathrm{TG}}{\mathrm{TG+FNG}} \cdot 100 \quad (3)$$

The Cohen's Kappa index (K) characterizes the map agreement with the ground truth after removing the chance factor. It is an indication of the adding value of the classification method, which is defined as ;

$$K = \frac{\text{overall accuracy - chance agreement}}{\text{1- chance agreement}} \quad (4)$$

where chance agreement is the probability of having a good classification by chance, which is derived from the ground truth and classification distribution.

3. Results

3.1 Calibration

The most important parameter is the smoothing parameter *(df)* whose effect is clearly illustrated in Figures 4-6. The goal of the smoothing is to remove signal oscillations that are not linked to mowing events (Figure 4). We observed that most of these undesirable oscillations correspond to short-term variations. Therefore, the smoothing should be strong enough to remove them (i.e $df < 15$) but should not be too strong as some mowing events might be missed (i.e $df = 5$). The calibration led to $df = 10$, which corresponds to an intermediate case in Figure 5. When applying the minimum detection on the smoothed LAI time serie we identified 3 events that are consistent with the mowing calendar (Figure 6). The rate of misclassified plots was about 13% after phase 1 (Table 3). The main source of error comes from the detection of NIG as IPG (9%) as shown in Figure 7.

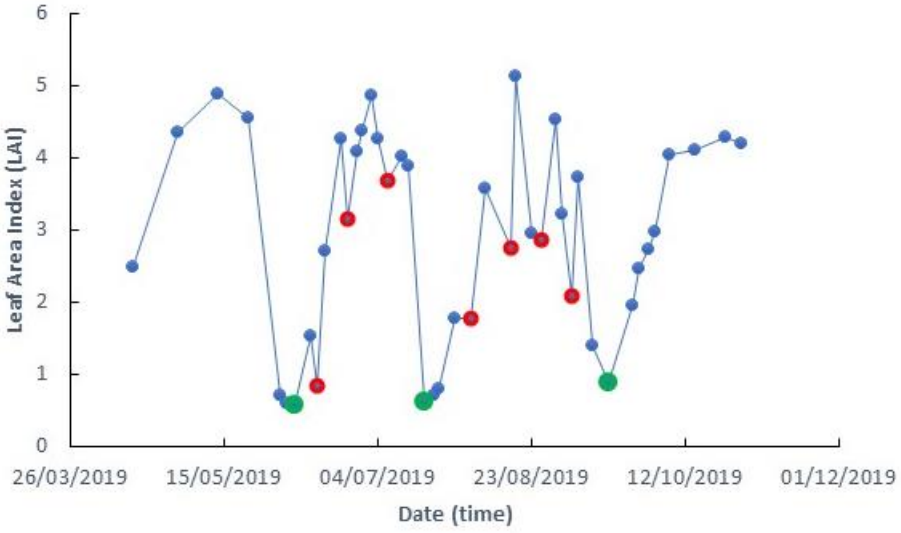

Figure 4 : raw LAI time series of an IPG pixel before smoothing, red dots correspond to LAI minimums that are not linked to mowing events. Green dots are LAI minimum linked to mowing event

Preprints (www.preprints.org) | NOT PEER-REVIEWED | Posted: 20 May 2022 doi:10.20944/preprints202205.0273.v1

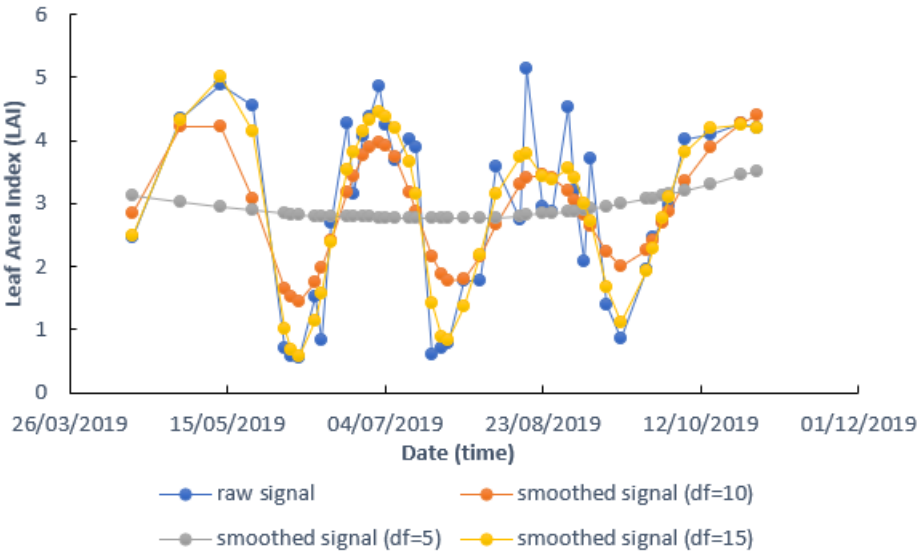

Figure 5 Effect of degrees of freedom (*df*) of the smoothed algorithms an a LAI times series of an IPG pixel.

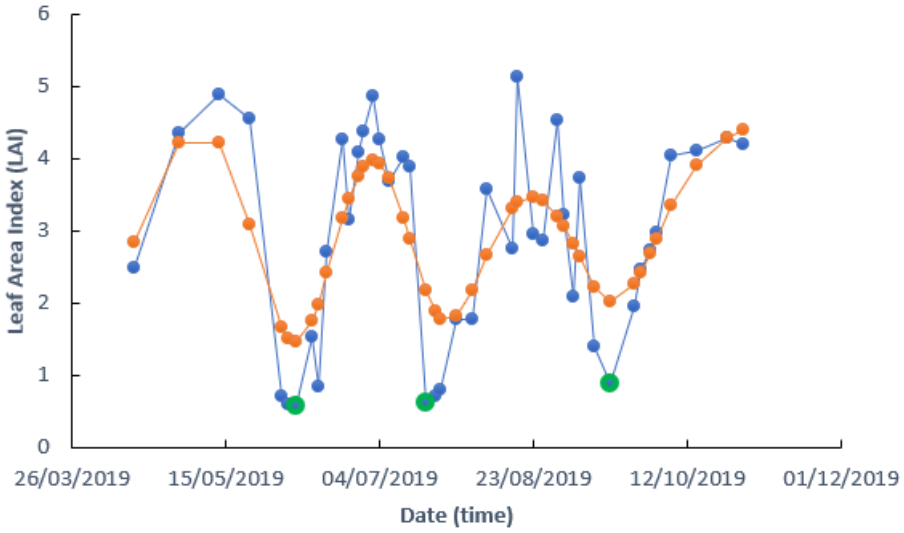

Figure 6 : raw LAI time series (blue) and smoothed LAI time series (orange) of an IPG pixel. Green dots correspond to minimum LAI detected on the smoothed LAI time series.

Preprints (www.preprints.org) | NOT PEER-REVIEWED | Posted: 20 May 2022 doi:10.20944/preprints202205.0273.v1

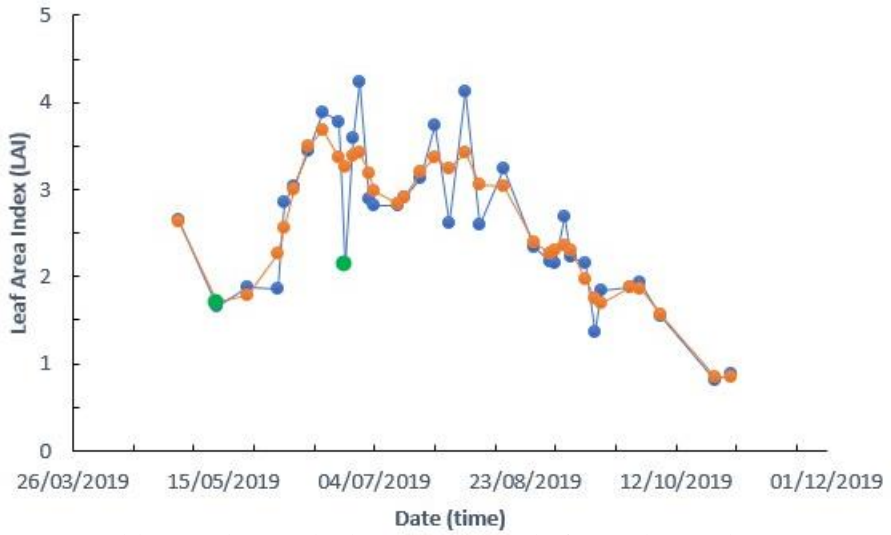

Figure 7 : raw (blue) and smoothed (orange) signal of NIG detected as an IPG

In the presented case the smoothing was not appropriate and some strong LAI oscillations were still present in the smoothed signal; thus, triggering the identification of false mowing events. However, the LAI values corresponding to the detected minimum were high and larger than what is expected with freshly mowed grass. An additional test on the LAI values at the detected minimum is a way to resolve the ambiguity displayed in Figure 7. The analysis of such errors led to defining the series of tests and data manipulation as described before in steps 3 and 4, which parameters were characterized in phase 2. After this phase, we reduced the misclassified plots rate to less than 4%, with still a greater probability to miss a NIG than a IPG (Table 3). The final values of the parameters of the algorithm are reported in Table 2. Most of them are likely generic while LAI thresholds and time windows could be linked to growth conditions. To illustrate the results of the algorithm, we selected an area covering two grassland plots surrounded by NIG area. The results obtained in 2019 are displayed in Figure 8 where letters represent the exact location of the pixel time series A, B and C displayed in Figures 9, 6 and 10, respectively. There is a clear difference in grass management with four mowing event in the nothern plot and three in the southern (Figure 8) as illustrated in Figures 10 and 6 If the plots are mostly homogeneous, some areas with less mowing events can be seen at the plot boarder, in the middle corresponding to a ditch bringing the water, and, in some patches. The case of point A (Figure 9) indicates that the missed last mowing event is explained by a low grass growth at end of the season. The difference between the minimum and the maximum after harvest was below 1.5 (*threshlai* < 1.5) reflecting less productive area that might be induced by soil properties or the quality of the irrigation with heterogeneities induced by a poor soil levelling.

Preprints (www.preprints.org) | NOT PEER-REVIEWED | Posted: 20 May 2022 doi:10.20944/preprints202205.0273.v1

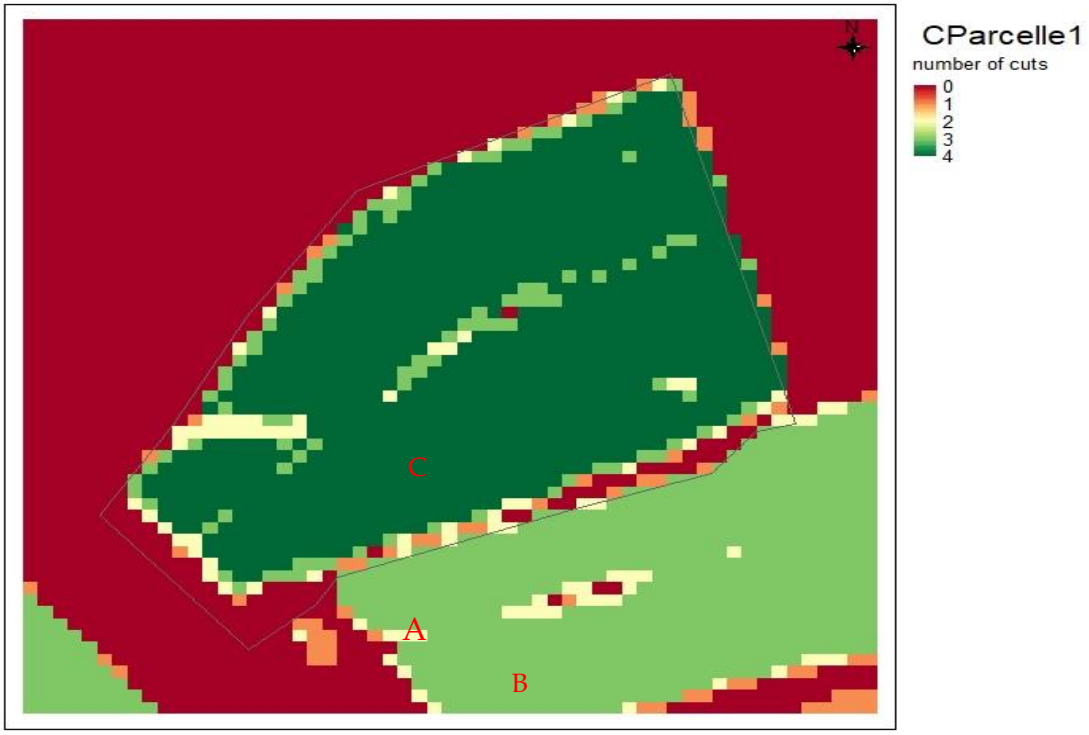

Figure 8: results obtained after the second phase of calibration in 2019 showing locations of Fig. 6, 9 and 10

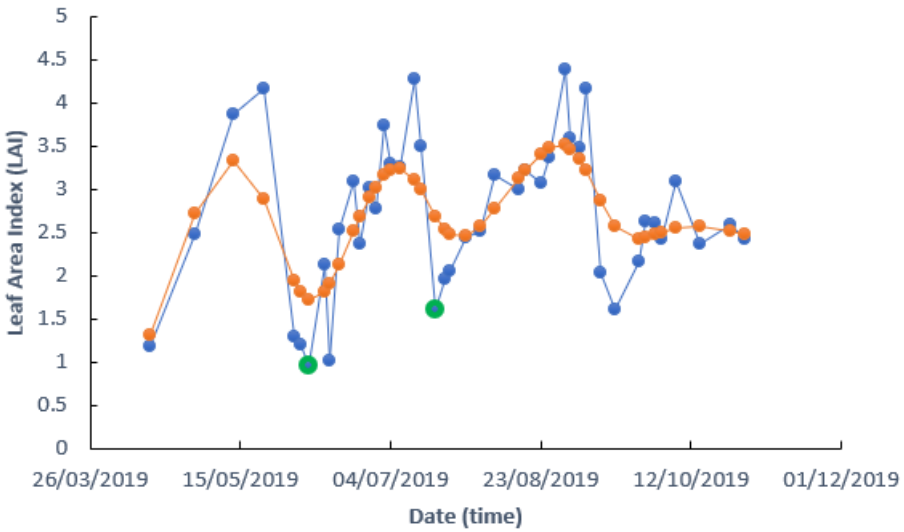

Figure 9: raw signal (blue) and smoothed signal (orange) of IPG showing two (2) mowing events with (green) dots).

Preprints (www.preprints.org) | NOT PEER-REVIEWED | Posted: 20 May 2022 doi:10.20944/preprints202205.0273.v1

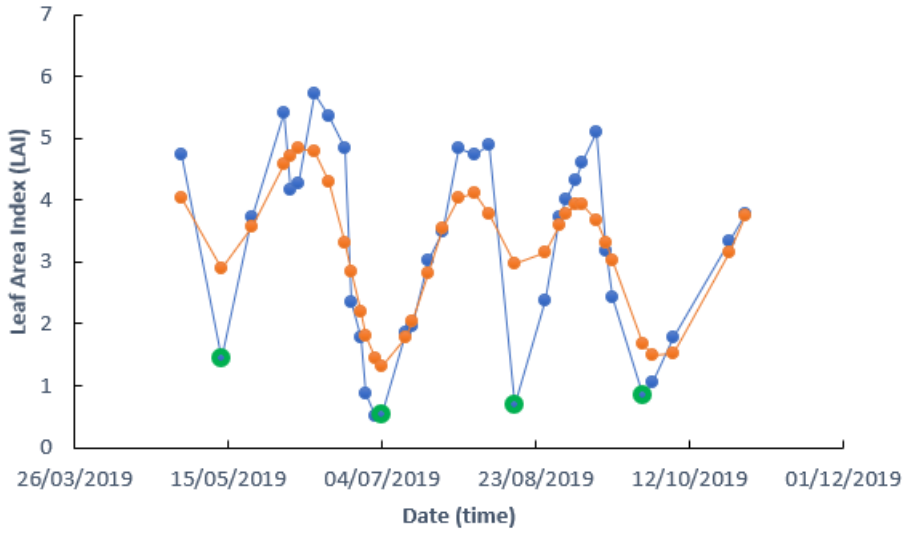

Figure 10 : raw (blue) and smoothed (orange) signal of IPG showing four (4) mowing events (green dots)

Evaluation results made on the validation data set results are given in Table 4. Excellent results were obtained with OA greater than 97% and a Kappa index between 0.94 and 0.99. The producer accuracy is equal to 100% for the NIG class, meaning that a parcel declared as a NIG is always NIG. This shows that the additional filtering can handle situations like the one shown in Figure 7. The producer's accuracies of the IPG class are a little less good, which means that some IPG plots are not detected. We will come back to this point in the discussion. There is also a year effect that appears clearly. For example, 2020 was the worst year, while the best results were obtained in 2018. The 2018 year is the wettest year during the summer, which may have limited the irrigation pressure and therefore allowed a good production throughout the cycle. In 2020 there was gap of 20 days in the measurements, which did not allow for the detection of the maximum grass development between the second and the third mowings, leading to miss these two events.

These good results have to be tempered by the fact that IPG are likely a class easy to detect as shown by the good results depicted in Table 4 with the other classification approaches (THEIA and SVM). However, our results are better than those obtained with the SVM method which means that algorithms based on artificial intelligence cannot necessarily capture the agronomic traits as used in our method. Although slightly better, our results are comparable to those of THEIA, which relies on a rich ground truth with the administrative census data (RPG database). The advantage of our method is that it does not require supervised learning even if some calibration was required on a few plots. We believe that the calibration is generic and that it can be used in other years and that the extension of our approach to other territories could be done based on an agronomic analysis of the agricultural practices, knowing that the parameters of our approach are all related to parameters that have a clear significance. Some of them are necessary to address times series with acquisition dates that are not optimal to detect mowing events while others are linked to well known agronomic features.

Table 2: List of parameters and value retained to implement the developed method

Parameters	**Definitions**	**Range of values used when calibrated**	**Final value**
fd	degree of freedom of the smoothing algorithm	5, 10, 15, 17	10

Preprints (www.preprints.org) | NOT PEER-REVIEWED | Posted: 20 May 2022 doi:10.20944/preprints202205.0273.v1

tlaimax	LAI threshold. a pixel is declared being not a grassland when the maximum of LAI time series is greater than *tlaimax*	10, 10.5, 11, 11.5	10.5
tlaimin	LAI threshold. A pixel is declared not to be a grassland when the maximum of the LAI time series is lower than tlaimin	4.0, 4.1, 4.2, 4.3, 4.4, 4.5	4.2
threshlai	LAI variation threshold before and after the detected minimum	0.5, 1.0, 1.5, 2.0, 2.5	1.5
dta1	Period to search for the true minimum after the smoothed minimum		15
dtb1	Period to search for the true minimum before the smoothed minimum		25
tlailow	LAI threshold to characterize unrealistic low LAI value		0.4
nbb	Number of points to consider in searching the maximum before a cut	2,4,6,8	4
dtmin1	Minimum time interval between observations bracketting the minimum leading to selecting the largest tminlai (tminlai1)		25
dtmin0	maximum time interval between observations bracketting the minimum leading to selecting the smallest tminlai (tminlai0)		10
tminlai1	largest LAI threshold to validate a minimum LAI (when time sampling is sparse)		2.5
tminlai0	smallest LAI threshold to validate a minimum LAI (when time sampling is frequent)		2
dta	Time before detecting a minimum		45
dtb	Time after detecting a minimum		45
difmax	The difference between the observed and the smoothed LAI above which the LAI is corrected.		2.6
Pixperc	The minimum rate of pixels detected as irrigated grass in a plot to classify it as an irrigated grass plot	50,70,90	90

Preprints (www.preprints.org) | NOT PEER-REVIEWED | Posted: 20 May 2022 doi:10.20944/preprints202205.0273.v1

Table 3: Calibration performance (score) after the first and second phases on the calibration data set. TG represents well-classified irrigated grassland polygons), FG, polygons classified as irrigated grassland while not an irrigated grassland, TNG, well classified not irrigated grassland polygons and FNG; irrigated grassland polygons classified as not irrigated grassland.

Calibration phases	Total plots	TG	TNG	FG	FNG
First calibration phase	748	372	281	69	26
Second calibration phase	748	416	304	25	3

Table 4: Summary of all the classification performances conducted in the Crau area.

Year	Overall accuracy	Producer's accuracy (IPG)	Producer's accuracy (NIG)	Kappa indice
Developed Classification				
Leaf Area Index (Sentinel-2) + proposed algorithm				
2016	97.7	95.2	100.0	0.96
2017	99.1	98.3	100.0	0.98
2018	99.7	99.4	100.0	0.99
2019	98.8	97.5	100.0	0.98
2020	96.9	93.8	99.7	0.94
THEIA Classification				
Satellite image + Land use data +Supervised classification				
2016	97.2	95.5	98.7	0.95
2017	98.6	96.9	100.0	0.97
2018	98.4	97.8	98.9	0.97
Classification via Support Vector Machine (SVM)				
Satellite images + supervised classification using SVM method				
2016	92.2	95.5	88.9	0.85
2017	94.1	96.9	91.5	0.89

SVM : support vector machine ; RPG : registre parcellaire graphique.

4. Discussion

The proposed method was applied to the whole territory of the Crau plain having 18058 plots with an illustration given in Figure 10 for the year 2018, showing all plots of IPG (in green) and NIG (in red). We do not have any reference on the whole territory and we can therefore only make relative analyses. In our discussion we would like to address 3 questions: i) what is the impact of classifying land use at plot scale compared to a pixel scale approach? ii) what is the evolution of irrigated areas between years and can it be linked to changes in land use? iii) At the territory scale, what are the differences between the areas classified as irrigated grassland with our method and that derived from the THEIA land use map?

Preprints (www.preprints.org) | NOT PEER-REVIEWED | Posted: 20 May 2022 doi:10.20944/preprints202205.0273.v1

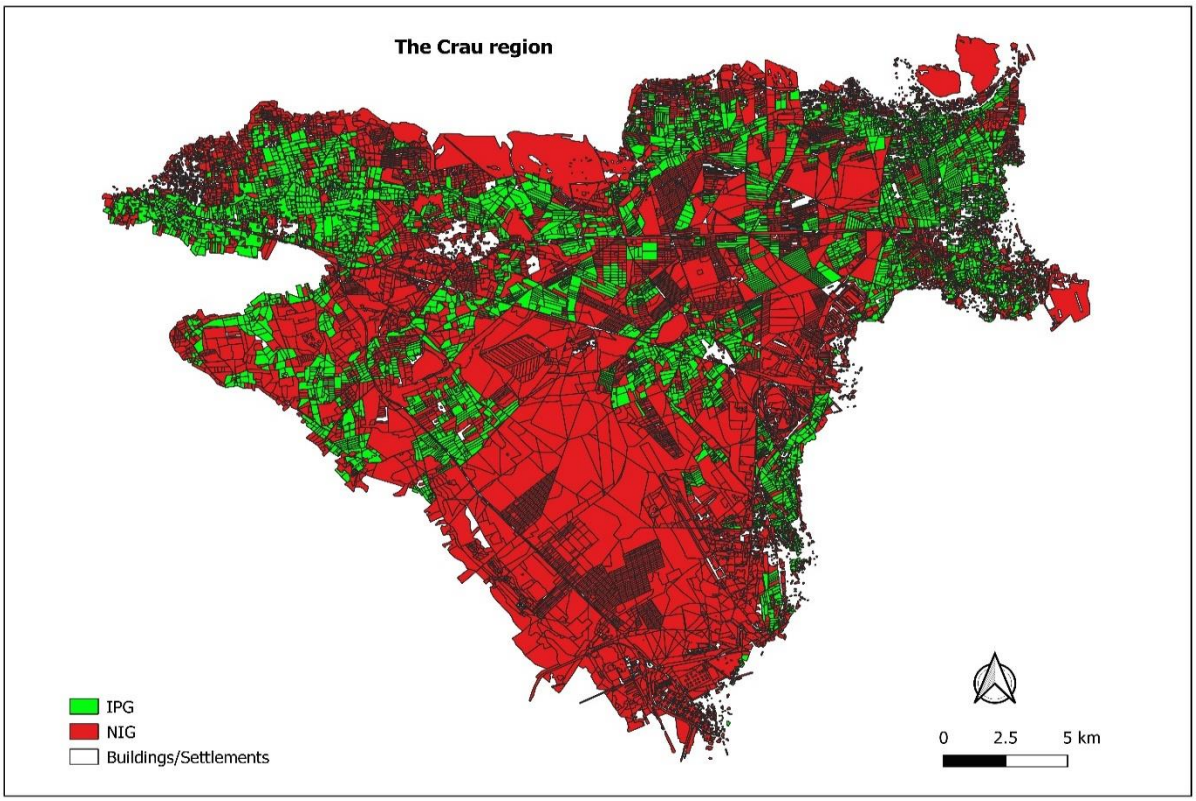

Fig 10 : Land use map using the developed algorithm in 2018

4.1 Impact of plot aggregation in the classification process

One of the constraints of the method applied in this work is that the land-use class is determined at the scale of a plot. The plot level is very important from an agronomic point of view and in particular for the characterisation of the irrigation. Indeed, with gravity irrigation as practiced on IPG, the quantities of water applied are dependent on the irrigated surface but also on the size of the plots, which conditions the average dose applied, the larger the plot, the higher the dose. We have seen in Figure 8 that the edges of the plot, the irrigation ditches within the plot, and certain less productive areas could lead to a lower number of mows and thus induce a misclassification of the pixel. It is also possible to have isolated pixels located in NIG areas that present several mowing-like events. Working at the plot level reduces the risk of error since the land-use class is based on a majority of pixels. However, a plot map with their boundaries is not always available, especially when large areas are considered. Furthermore, the plot map may contain errors generating errors in the areas counted or misclassification of an IPG plot when it includes a significant part (>10% in our case) of an area that is not an IPG.

To assess the impact of the classification method, we present in Table 4 the areas detected as IPG using 1) a plot aggregation approach to validate the belonging to the IPG class and 2) a pixel based approach by calculating the area of all pixels presenting two (2) or more mowing events. The pixels of the study site (the Crau) were obtained by considering those within an extraction polygon that is as close as possible to the considered area being the aggregation of plots. As this area present sometimes a bit complex boundary (Figure 10), the extracted polygon was drawn inside the area explaining the total areas of the pixel based and plot base counting are a bit different (Table 5). The percentages

Preprints (www.preprints.org) | NOT PEER-REVIEWED | Posted: 20 May 2022 doi:10.20944/preprints202205.0273.v1

of IPG based on the aggregation approach ranged from 25-26% and 74-75% for NIG while for the pixel approach the percentages of IPG ranged from 22-25% and 75-78% for the NIG. According to the year, differences between 1.3% and 3.9% in IPG surface are found between the classification made at the plot scale (aggregation method) and that made at pixel scale (pixel approach) with the aggregation method always higher. The underestimation obtained with the pixel-based approach, likely due to plot boarder effect, remained however moderate.

Table 5: Total surfaces obtained for IPG and NIG classes using the developped classification algorithm obtained with a plot aggregation or a pixel based approaches

Plot aggregation approach			
	IPG	**NIG**	**Total plots**
2016	13318 ha	40264 ha	53581 ha
2017	13717 ha	39864 ha	53581 ha
2018	13839 ha	39742 ha	53581 ha
2019	13994 ha	39587 ha	53581 ha
2020	13850 ha	39731 ha	53581 ha
Pixel approach			
	IPG	**NIG**	**Total pixels**
2016	11480 ha	40520 ha	52000ha
2017	11770 ha	40230 ha	52000 ha
2018	12345 ha	39655 ha	52000 ha
2019	11561 ha	40439 ha	52000 ha
2020	12758 ha	39242 ha	52000 ha

4.2 Ability to detect land-use changes

The proposed method implemented across the five years (2016-2020) gave us an overview of the consistency of the results from one year to another. Results are displayed in Table 6 by considering plots where the classification remain stable over the five years (i.e GGGGG and NNNNN classes), plots that met one change that can be attributed to a land-use change, and plot having several changes reflecting problems in their classification. In 91% of the case, perfect stability was observed. The analysis was made on plots presenting one change with spatial illustrations depicted in Figure 11. The figure shows that changes are spread over the area with plot of different sizes. The causes of the change were identified by analysing the high-resolution images acquired during the considered period. From these images we can identify the following key features clearly:

- LUC: land-use change most of them being IPG converted in urban areas, orchards or abandon and vice versa
- EXPL: some plots have been levelled and resown, the algorithm can fail to acknowledge such plots as IPG, especially for the first year because there is relatively very low vegetation growth.
- MGT: Some plots are very heterogeneous likely due to permanent grazing or irrigations problems such as the insufficient flow of irrigation water or a lack of levelling preventing a homogeneous water supply.

In the other cases, hereafter labelled as ERR, there were no clear features that can explain the classification change during the considered period.

Preprints (www.preprints.org) | NOT PEER-REVIEWED | Posted: 20 May 2022 doi:10.20944/preprints202205.0273.v1

Table 6: Composition of land-use change classes. (The Land-use type sequence corresponds to the five-year succession G and N corresponding to the IPG and NIG classes, respectively).

Case ID	Land-use type	Sources of variations	Number of plots >1 ha
Consistent classification through the 5 years			
1	G G G G G		3156
2	N N N N N		6623
Plots presenting one land-use change through the 5 years			
3	G G G G N	MGT (60); ERR (15)	75
4	G G G N N	MGT (34); LUC (15); EXPL (10)	59
5	G G N N N	MGT(40); LUC (40); EXPL (20);	100
6	G N N N N	MGT (21); EXPL (6); LUC (10)	37
7	N G G G G	MGT (139); EXPL (14); ERR (32)	185
8	N N G G G	MGT (27); LUC (7); EXPL(11); ERR (5)	50
9	N N N G G	MGT (20); ERR (5); LUC(6)	31
10	N N N N G	MGT (47); LUC (20); EXPL (3)	70
Plots presenting ≥ 2 land-use changes through the 5 years			
11	G N G N G	MGT(65); EXPL (25); ERR (10)	100
12	All plots		331

G=grassland; N=non-grassland.

Analysis of the data in the table 6 shows that over the 5 years, 607 (6%) show one change in classification while 331 (3%) show at least two changes. The analysis of the high-resolution images on plots with time series presenting at least one change shows that when a plot is detected as an IPG it is always an IPG. On the 707 plots controlled, only one case corresponding to a young grassed orchard generated an error. This confirms the reliability of the algorithm when an IPG is detected as shown in table 4 with a producer accuracy close to 100% which reflects the absence of detected IPG while NIG. Of all the plots with at least one year classified as IPG (class Id 1, 3-10, 11 in Table 6), 19% have discontinuous NIG-IPG series over the 5 years. These plots are mostly related to heterogeneity problems (MGT) (66% of the cases) while in 27% of the cases a real change in use (LUC) or a plot levelling (EXPL) was observed. If we consider the cases where the change is confirmed over the last 2 or 3 years, the cumulative rate of LUC and EXPL features increased to 50%.

This leads us to conclude that the use of long series (5 years) allows us to characterise the IPGs even when they present strong heterogeneities linked to irrigation defects or grazing during the summer period. The occurrence of IPG detection could be a marker of grassland management and might be used as an information to refine the desciption of grassland systems. Detection of real land-use change needs confirmation of the change over several years (> 3 years) which requires time series longer than 5 years to reduce the ambiguity between actual land use change and classification errors induced by grassland management.

Preprints (www.preprints.org) | NOT PEER-REVIEWED | Posted: 20 May 2022 doi:10.20944/preprints202205.0273.v1

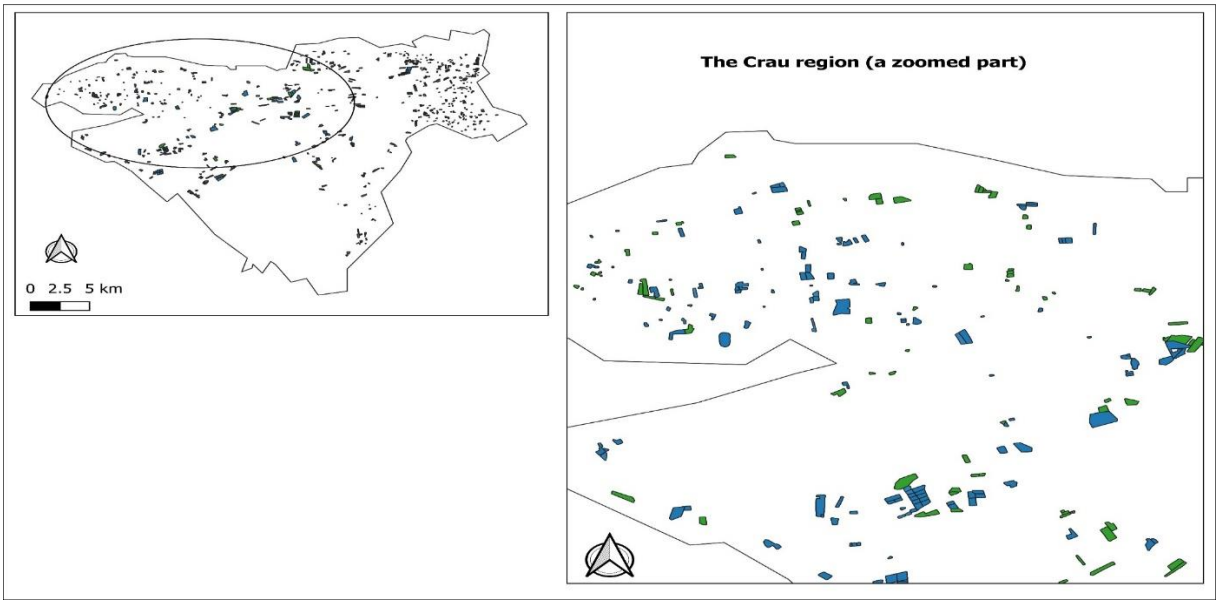

Figure 11 : Landuse change map 2016-2020 showing changes from IPG to NIG (green) and NIG to IPG (blue) with a zoomed part

4.3 comparison with the THEIA product at the territory scale

Further comparisons were made between the THEIA land-use classification against our developed classification for the three different years separately as shown in Table 7. The rate of plots classified differently between the two classification methods ranged between 3.7 and 4.9% of the total number of plots larger than 1 ha. Despite the slight differences in the Kappa index between THEIA and our developed classification (Table 4), it can be seen in Table 7 that discrepencies were found over 9% of the plots.

The two types of differences IPG (Developed) – NIG (THEIA) and NIG(Developed)-IPG (THEIA) must be interpreted differently. When the plots were classified as IPG by the developed method, we found in the previous section that the chance of having a real IPG is very high thus indicating that the THEIA algorithm is failing when indicating a NIG (e.g in 77 plots in 2016). However, the number of plots falling in that case, is lower than the reverse difference when an IPG is detected by THEIA. A random subset of 25 plots seen in 2016 as IPG by THEIA and NIG by the developed method was analysed on high-resolution images to identify the discrepancy origins. Eleven plots (44%) corresponded to very heterogenous IPG plots and/or plots submitted to permanent grazing. In that case we can conclude that the developed method failed to classify the plots. Eleven plots (44%) corresponded to a land-use error with urban plots with gardens, field crops, or humid ecosystems. With the last 3 plots (12%), there is an obvious problem of plot boundary including two or more surface types. In these two latter cases we can conclude that THEIA method failed to classify the plots. With THEIA a plot is classified when grassland is the dominant land use, while the threshold with our classification requires that 90% of the plot's pixels present at least two mowing events. Therefore, the THEIA approach can detect IPG in much more heterogeneous situations than with our developed method. These results tend to show a certain superiority of the developed classification when counting the misclassified plots for each method: 448 x 0.44 = 197 plots with the developed method and 77 + 0.56 x 448 = 328 plots with the THEAI method These results obtained in 2016 are even more advantageous for the developed method for the other years.

Preprints (www.preprints.org) | NOT PEER-REVIEWED | Posted: 20 May 2022 doi:10.20944/preprints202205.0273.v1

Table 7: comparison of plot classification disagreement between the developed classification (Dev) and Theia classification (THEIA) for both individual and combined years

Years	IPG (Dev) – NIG (THEIA)	NIG(Dev)-IPG(THEIA)	Total nb plots> 1ha (rate of difference)
2016	77	448	10739 (4.9%)
2017	109	287	10739 (3.7%)
2018	149	333	10739 (4.5%)
	Number of plots with more than1 difference		
2016-2018	976		10739 (9.1%)

5. Conclusions

A new algorithm for the identification of Irrigated Permanent Grass (IPG) was developed in this study. It is based on the detection of agronomic traits thanks to the possibility offered by the Sentinel 2 mission to provide frequent images of the vegetation development. In our area located in the Mediterranean about 40 images per year can be exploited during the period of interest (mid-April to October ending). IPGs were classified by detecting mowing events assuming that a pixel is an IPG when at least two mowing events were detected. The developed classification method offers very good results, better than that obtained when using SVM or RF methods as used in the THEIA approach. The method presents the advantage of not depending on training samples, even if some calibration was necessary to fix some thresholds and deal with the remote sensing signal noise. We believe that calibration effort will likely be lower when addressing IPG detection in other geographical contexts. Moreover, once established the algorithm can be applied directly to another year.

Despite the good performance of the developed algorithm, it is faced with some constraints that lead to failure to detect mowing activities. For instance, when there is relatively very low biomass or a heterogeneous plot, the developed algorithm tends to fail by missing some mowing events. This can be seen as a weakness, but our analysis has shown that the IPG class covers several management modalities. Depending on the objectives, such a weakness can be a strength to characterize different production systems. In addition, the detection of mowing should make it possible to understand the technical itineraries and to provide information do inform the farming practice heterogeneities over large territory to implement crop models. Real changes in use can be observed, but long time series are needed to confirm the change and remove ambiguities with heterogeneous grasslands.

In general, one can question the relevance of relying on agronomic traits specific to certain types of land use to map them. In this work, we have relied on a clear, specific, and somewhat caricatural trait and this has allowed excellent results. The results in the literature are not necessarily as precise, probably due to less clear specific features that can lead to ambiguities. We believe, for example, that the separation of vineyards and orchards, which is important to map different irrigation strategies, may be more difficult to characterize. Moreover, it was found that the method requires frequent acquisition to catch the events of interests. For locations with frequent cloud cover, combining optic and radar images can be an option to overcome the lack of optical data.

Acknowledgments

This work was funded by Petroleum Technology Development Fund (PTDF) under the Federal Ministry of Petroleum, Nigeria, in collaboration with INRAE-EMMAH Avignon as part of a PhD research program.

References

(1) United Nations. *International Decade for Action on Water for Sustainable Development, 2018-2028* ***2016***. https://www.un.org/en/events/waterdecade/background.shtml (accessed 2022-04-14).

(2) Wriedt, G.; Van der Velde, M.; Aloe, A.; Bouraoui, F. Estimating Irrigation Water Requirements in Europe. *Journal of Hydrology* **2009**, *373* (3), 527–544. https://doi.org/10.1016/j.jhydrol.2009.05.018.

(3) Wada, Y.; Wisser, D.; Eisner, S.; Flörke, M.; Gerten, D.; Haddeland, I.; Hanasaki, N.; Masaki, Y.; Portmann, F. T.; Stacke, T.; Tessler, Z.; Schewe, J. Multimodel Projections and Uncertainties of Irrigation Water Demand under Climate Change. *Geophysical Research Letters* **2013**, *40* (17), 4626–4632. https://doi.org/10.1002/grl.50686.

(4) Marras, P. A.; Lima, D. C. A.; Soares, P. M. M.; Cardoso, R. M.; Medas, D.; Dore, E.; De Giudici, G. Future Precipitation in a Mediterranean Island and Streamflow Changes for a Small Basin Using EURO-CORDEX Regional Climate Simulations and the SWAT Model. *Journal of Hydrology* **2021**, *603*, 127025. https://doi.org/10.1016/j.jhydrol.2021.127025.

(5) Bazzi, H.; Baghdadi, N.; Ienco, D.; El Hajj, M.; Zribi, M.; Belhouchette, H.; Jose Escorihuela, M.; Demarez, V. Mapping Irrigated Areas Using Sentinel-1 Time Series in Catalonia, Spain. *Remote Sens.* **2019**, *11* (15), 1836. https://doi.org/10.3390/rs11151836.

(6) Gao, Q.; Zribi, M.; Escorihuela, M.; Baghdadi, N.; Segui, P. Irrigation Mapping Using Sentinel-1 Time Series at Field Scale. *Remote Sensing* **2018**, *10* (9), 1495. https://doi.org/10.3390/rs10091495.

(7) Ambika, A. K.; Wardlow, B.; Mishra, V. Remotely Sensed High Resolution Irrigated Area Mapping in India for 2000 to 2015. *Sci. Data* **2016**, *3*, 160118. https://doi.org/10.1038/sdata.2016.118.

(8) Massari, C.; Modanesi, S.; Dari, J.; Gruber, A.; De Lannoy, G. J. M.; Girotto, M.; Quintana-Segui, P.; Le Page, M.; Jarlan, L.; Zribi, M.; Ouaadi, N.; Vreugdenhil, M.; Zappa, L.; Dorigo, W.; Wagner, W.; Brombacher, J.; Pelgrum, H.; Jaquot, P.; Freeman, V.; Volden, E.; Prieto, D. F.; Tarpanelli, A.; Barbetta, S.; Brocca, L. A Review of Irrigation Information Retrievals from Space and Their Utility for Users. *Remote Sens.* **2021**, *13* (20), 4112. https://doi.org/10.3390/rs13204112.

(9) Ozdogan, M.; Gutman, G. A New Methodology to Map Irrigated Areas Using Multi-Temporal MODIS and Ancillary Data: An Application Example in the Continental US. *Remote Sensing of Environment* **2008**, *112* (9), 3520–3537. https://doi.org/10.1016/j.rse.2008.04.010.

(10) Deines, J. M.; Kendall, A. D.; Hyndman, D. W. Annual Irrigation Dynamics in the US Northern High Plains Derived from Landsat Satellite Data. *Geophys. Res. Lett.* **2017**, *44* (18), 9350–9360. https://doi.org/10.1002/2017GL074071.

(11) Demarez, V.; Helen, F.; Marais-Sicre, C.; Baup, F. In-Season Mapping of Irrigated Crops Using Landsat 8 and Sentinel-1 Time Series. *Remote Sens.* **2019**, *11* (2), 118. https://doi.org/10.3390/rs11020118.

(12) Pageot, Y.; Baup, F.; Inglada, J.; Baghdadi, N.; Demarez, V. Detection of Irrigated and Rainfed Crops in Temperate Areas Using Sentinel-1 and Sentinel-2 Time Series. *Remote Sens.* **2020**, *12* (18), 3044. https://doi.org/10.3390/rs12183044.

(13) Bazzi, H.; Baghdadi, N.; Amin, G.; Fayad, I.; Zribi, M.; Demarez, V.; Belhouchette, H. An Operational Framework for Mapping Irrigated Areas at Plot Scale Using Sentinel-1 and Sentinel-2 Data. *Remote Sensing* **2021**, *13* (13), 2584. https://doi.org/10.3390/rs13132584.

(14) Karantzalos, K.; Karmas, A.; Tzotsos, A. Monitoring Crop Growth and Key Agronomic Parameters through Multitemporal Observations and Time Series Analysis from Remote Sensing Big Data. *Advances in Animal Biosciences* **2017**, *8* (2), 394–399. https://doi.org/10.1017/S2040470017001261.

(15) Ashourloo, D. Automatic Canola Mapping Using Time Series of Sentinel 2 Images. *ISPRS Journal of Photogrammetry and Remote Sensing* **2019**, 14.

(16) Ashourloo, D.; Shahrabi, H. S.; Azadbakht, M.; Rad, A. M.; Aghighi, H.; Radiom, S. A Novel Method for Automatic Potato Mapping Using Time Series of Sentinel-2 Images. *Computers and Electronics in Agriculture* **2020**, *175*, 105583. https://doi.org/10.1016/j.compag.2020.105583.

(17) Julien, Y.; Sobrino, J. A.; Jiménez-Muñoz, J.-C. Land Use Classification from Multitemporal Landsat Imagery Using the Yearly Land Cover Dynamics (YLCD) Method. *International Journal of Applied Earth Observation and Geoinformation* **2011**, *13* (5), 711–720. https://doi.org/10.1016/j.jag.2011.05.008.

(18) Merot, A.; Bergez, J.-E.; Capillon, A.; Wery, J. Analysing Farming Practices to Develop a Numerical, Operational Model of Farmers' Decision-Making Processes: An Irrigated Hay Cropping System in France. *Agricultural Systems* **2008**, *98* (2), 108–118. https://doi.org/10.1016/j.agsy.2008.05.001.

(19) Dusseux, P.; Vertes, F.; Corpetti, T.; Corgne, S.; Hubert-Moy, L. Agricultural Practices in Grasslands Detected by Spatial Remote Sensing. *Environ. Monit. Assess.* **2014**, *186* (12), 8249–8265. https://doi.org/10.1007/s10661-014-4001-5.

(20) Gómez Giménez, M.; de Jong, R.; Della Peruta, R.; Keller, A.; Schaepman, M. E. Determination of Grassland Use Intensity Based on Multi-Temporal Remote Sensing Data and Ecological Indicators. *Remote Sensing of Environment* **2017**, *198*, 126–139. https://doi.org/10.1016/j.rse.2017.06.003.

(21) Stumpf, F.; Schneider, M. K.; Keller, A.; Mayr, A.; Rentschler, T.; Meuli, R. G.; Schaepman, M.; Liebisch, F. Spatial Monitoring of Grassland Management Using Multi-Temporal Satellite Imagery. *Ecol. Indic.* **2020**, *113*, 106201. https://doi.org/10.1016/j.ecolind.2020.106201.

(22) Courault, D.; Hadria, R.; Ruget, F.; Olioso, A.; Duchemin, B.; Hagolle, O.; Dedieu, G. Combined Use of FORMOSAT-2 Images with a Crop Model for Biomass and Water Monitoring of Permanent Grassland in Mediterranean Region. *Hydrology and Earth System Sciences* **2010**, *14* (9), 1731–1744. https://doi.org/10.5194/hess-14-1731-2010.

(23) Schwieder, M.; Wesemeyer, M.; Frantz, D.; Pfoch, K.; Erasmi, S.; Pickert, J.; Nendel, C.; Hostert, P. Mapping Grassland Mowing Events across Germany Based on Combined Sentinel-2 and Landsat 8 Time Series. *Remote Sensing of Environment* **2022**, *269*, 112795. https://doi.org/10.1016/j.rse.2021.112795.

(24) Séraphin, P.; Vallet-Coulomb, C.; Gonçalvès, J. Partitioning Groundwater Recharge between Rainfall Infiltration and Irrigation Return Flow Using Stable Isotopes: The Crau Aquifer. *Journal of Hydrology* **2016**, *542*, 241–253. https://doi.org/10.1016/j.jhydrol.2016.09.005.

(25) Weiss, M.; Baret, F.; Leroy, M.; Hautecoeur, O.; Bacour, C.; Prevot, L.; Bruguier, N. Validation of Neural Net Techniques to Estimate Canopy Biophysical Variables from Remote Sensing Data. *Agronomie* **2002**, *22* (6), 547–553. https://doi.org/10.1051/agro:2002036.

(26) Inglada, J.; Vincent, A.; Arias, M.; Tardy, B.; Morin, D.; Rodes, I. Operational High Resolution Land Cover Map Production at the Country Scale Using Satellite Image Time Series. *Remote Sens.* **2017**, *9* (1), 95. https://doi.org/10.3390/rs9010095.

(27) De Vroey, M.; Radoux, J.; Defourny, P. Grassland Mowing Detection Using Sentinel-1 Time Series: Potential and Limitations. *Remote Sens.* **2021**, *13* (3), 348. https://doi.org/10.3390/rs13030348.

(28) Tian, J.; Zhu, X.; Chen, J.; Wang, C.; Shen, M.; Yang, W.; Tan, X.; Xu, S.; Li, Z. Improving the Accuracy of Spring Phenology Detection by Optimally Smoothing Satellite Vegetation Index Time Series Based on Local Cloud Frequency. *ISPRS Journal of Photogrammetry and Remote Sensing* **2021**, *180*, 29–44. https://doi.org/10.1016/j.isprsjprs.2021.08.003.

(29) Hastie, T. J, and Tibshirani R. J. *Generalized additive models*. Chapman and Hall/CRC, **1990**, ISBN 978-0-412-34390-2.

(30) Congalton, R. G. Accuracy Assessment and Validation of Remotely Sensed and Other Spatial Information. *International Journal of Wildland Fire* **2001**, *10* (3–4), 321–328. https://doi.org/10.1071/WF01031.